eprints@whiterose.ac.uk
https://eprints.whiterose.ac.uk/

Directional Modulation Design under a Given Symbol-Independent Magnitude Constraint for Secure IoT Networks

Bo Zhang, *Member, IEEE,* Wei Liu, *Senior Member, IEEE,* Qiang Li, Yang Li, Xiaonan Zhao, Cuiping Zhang and Cheng Wang

Abstract—Directional modulation (DM) is an important technology for physical layer security in wireless communications. Recently, a symbol-independent magnitude constraint for all antennas was proposed in DM design to reduce the design complexity of its analogue implementation. However, a limitation of the method is that it can only set the magnitude to a certain value, and all the antenna coefficients have the same magnitude. In this paper, a more flexible solution is provided and the challenge of the design is the non-convex constraint enforcing an arbitrary symbol-independent magnitude for all coefficients. To solve the problem, a convex iterative method is proposed, based on which the magnitudes of weight coefficients for all antennas can be chosen by designers in advance according to the specific requirements, allowing more freedom in the design process, which is the major difference between the previously proposed design and the newly proposed one. Two design examples are provided to demonstrate the effectiveness of the proposed design. One is is a general example, where coefficient magnitudes for different symbols are the same for the same antenna, but different for different antennas; the other one is a special case where magnitudes for all antennas are the same.

Keywords: Directional modulation, symbol-independent magnitude, non-convex optimisation, antenna arrays.

I. INTRODUCTION

With the fast evolution of wireless communication systems, 6G enabled IoT (Internet of Things) has attracted extensive attention in both academia and industry. The IoT is expected to give massive connectivity and exchange of information through wireless communication among different things, such as sensors, mobile phones and vehicles [1–4]. Due to its broadcasting characteristics, undesired receivers may be able to receive the useful information with high sensitivity eavesdroppers. Therefore, high reliability and stability of the communication link is necessary [5]. Beamforming has been used to amplify signal power while avoding eavesdroppers and widely studied for IoT sensor networks [6–8]. Recently,

Bo Zhang, Xiaonan Zhao, Yang Li, Cuiping Zhang and Cheng Wang are with Tianjin Key Laboratory of Wireless Mobile Communications and Power Transmission, College of Electronic and Communication Engineering, Tianjin Normal University, 300387, China.

Wei Liu is with the Communications Group, Department of Electronic and Electrical Engineering, University of Sheffield, Sheffield, S1 3JD, UK.

Qiang Li is with the College of Information Engineering, Shenzhen University, Shenzhen, 518060, China.

directional modulation (DM) as a beamforming based technology has received significant attention with its ability to keep a known modulation scheme to the desired direction or directions but scramble the pattern in other directions [9–23]. In [24], with the same transmitting power, static and dynamic jamming signals were both added to the transmitter for better security performance. In [25], particle swarm optimization was introduced to a phased antenna array to optimize the values of weight coefficients for reducing the beam width of directional modulation transmitted signal. In [26], directional modulation was extended from additive white Gaussian noise channel to multipath fading channel, further expanding the scope of application. In [27, 28], based on the retrodirective antenna array, a spatial technique was proposed to make the transmitted signal directional for improved physical layer security.

In the current DM design, for a transmitting antenna array, because the weight coefficient corresponding to each antenna is a complex number, when implemented by analogue circuits, both magnitude and phase responses of the feed circuits will be different for different antennas and different symbols, which will increase the implementation complexity of the whole system. To solve the problem, a symbol-independent magnitude constraint for all antennas was proposed in DM design recently [29]. However, a limitation with the method is that it can only set the magnitude to be a certain value, and the change of magnitude will result in the change of beam responses. In this paper, a constant magnitude constraint is proposed, which allows an effective phase-only control of the directional modulation system, while the amplification ratio of the radio frequency circuits can be fixed. Moreover, different from a previously proposed design, the magnitudes of weight coefficients for all antennas can be chosen by designers in advance according to the specific requirements, allowing more freedom in the design process.

The remaining part of this paper is structured as follows. A review of DM design based on a linear antenna array is given in Sec. II. A convex iterative solution to the given symbol-independent magnitude constraint for all antennas is proposed in Sec. III. Design examples are provided in Sec. IV, followed by conclusions in Sec. V.

II. REVIEW OF DM DESIGN BASED ON A LINEAR ANTENNA ARRAY

As shown in Fig. 1, the transmitter includes N antennas and the distance between the zeroth and the n-th antenna is
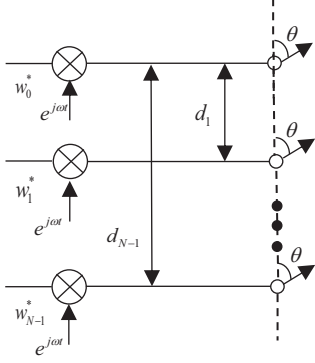
Fig. 1. DM design based on a linear antenna array.

represented by d_n ($n = 1, 2, \ldots, N-1$), with the transmission angle $\theta \in [0°, 180°]$. The weight coefficient for the n-th antenna is represented by w_n ($n = 0, 1, \ldots, N-1$). The steering vector of the array is given by [30]

$$\mathbf{s}(\omega, \theta) = [1, e^{j\omega d_1 \cos\theta/c}, \ldots, e^{j\omega d_{N-1} \cos\theta/c}]^T, \quad (1)$$

where the superscript T indicates the transpose operation, and $\tau_n = \frac{d_n \cos(\theta)}{c}$ is the time advance between the zeroth and n-th antennas. Weight coefficients for all antennas can be gathered together to form a vector

$$\mathbf{w} = [w_0, w_1, \ldots, w_{N-1}]^T. \quad (2)$$

Then, the beam response is given by

$$p(\omega, \theta) = \mathbf{w}^H \mathbf{s}(\omega, \theta), \quad (3)$$

where the superscript H represents Hermitian transpose.

For M-ary signaling, $p_m(\omega, \theta)$ represents the desired array response for the m-th symbol ($m = 0, \ldots, M-1$), with the corresponding weight vector

$$\mathbf{w}_m = [w_{m,0}, \ldots, w_{m,N-1}]^T. \quad (4)$$

Assume r directions are included in desired directions and $R-r$ directions are in un-desired directions. Then, the desired responses for the m-th symbol can be divided into two parts

$$\begin{aligned}
\mathbf{p}_m(\omega, \theta_{SL}) =& [p_m(\omega, \theta_0), p_m(\omega, \theta_1), \ldots, p_m(\omega, \theta_{R-r-1})], \\
\mathbf{p}_m(\omega, \theta_{ML}) =& [p_m(\omega, \theta_{R-r}), p_m(\omega, \theta_{R-r+1}), \ldots, \\
& \qquad p_m(\omega, \theta_{R-1})] .
\end{aligned} \quad (5)$$

Similarly, we can construct $\mathbf{S}(\omega, \theta_{SL})$ and $\mathbf{S}(\omega, \theta_{ML})$ as steering matrices in the un-desired directions and the desired directions, respectively. Then, for the DM design, the weight coefficient for the m-th symbol can be calculated by

$$\begin{aligned}
\min_{\mathbf{w}_m} \quad & ||\mathbf{p}_m(\omega, \theta_{SL}) - \mathbf{w}_m^H \mathbf{S}(\omega, \theta_{SL})||_2 \\
\text{subject to} \quad & \mathbf{w}_m^H \mathbf{S}(\omega, \theta_{ML}) = \mathbf{p}_m(\omega, \theta_{ML}).
\end{aligned} \quad (6)$$

III. A CONSTANT SYMBOL-INDEPENDENT MAGNITUDE CONSTRAINT FOR ALL ANTENNAS

However, the magnitudes of weight coefficients calculated by (6) for all antennas and M symbols are not the same; in

other words, for the DM design in wireless communications, an individual tailor-made feed circuit is needed for each antenna and symbol for analogue implementation, increasing the complexity of the design. In this section, we propose a new method to realize the constant symbol-independent magnitude constraint to ensure that each antenna's coefficient has the same magnitude for different symbols, and compared with the method proposed in [29], the new solution can help set the amplitude values of weight coefficients arbitrarily in advance according to designers' requirements. Mathematically, the above description can be expressed as

$$|\mathbf{w}_m| = \mathbf{\Gamma}, \quad (7)$$

where $|\cdot|$ represents element-wise absolute value operation, $\mathbf{\Gamma}$ is a $1 \times N$ vector, given by

$$\mathbf{\Gamma} = [\gamma_0, \gamma_1, \ldots, \gamma_{N-1}], \quad (8)$$

with $\gamma_n, n = 0, 1, \ldots, N-1$ being the required coefficient magnitude for corresponding antennas.

Then, the DM design with the proposed magnitude constraint for the m-th symbol can be formulated as

$$\begin{aligned}
\min_{\mathbf{w}_m} \quad & ||\mathbf{p}_m(\omega, \theta_{SL}) - \mathbf{w}_m^H \mathbf{S}(\omega, \theta_{SL})||_2 \\
\text{subject to} \quad & \mathbf{w}_m^H \mathbf{S}(\omega, \theta_{ML}) = \mathbf{p}_m(\omega, \theta_{ML}), |\mathbf{w}_m| = \mathbf{\Gamma}.
\end{aligned} \quad (9)$$

However, (9) is nonconvex due to the magnitude equality constraint. In previous design [29], through setting $\mathbf{\Gamma}$ as the vector of the minimum values of weight coefficients, the nonconvex problem can be transformed into a convex problem and it is easy to be solved by existing optimisation toolboxes. However, all elements in $\mathbf{\Gamma}$ have to be set to the same value, and it is not suitable for practical applications where different factors may affect the performances of different radio frequency circuits. To solve the problem, in this paper, we introduce a set of auxiliary parameters $\mathbf{k}_m$ (a $1 \times N$ vector) where $\mathbf{k}_m = \angle\mathbf{w}_m$ (the angle of $\mathbf{w}_m$). Then, $|\mathbf{w}_m|$ can be broken down into

$$|\mathbf{w}_m| = \mathbf{w}_m \cdot e^{-j\mathbf{k}_m} = \mathbf{\Gamma}, \quad (10)$$

where $\cdot$ represents element-wise multiplication. Based on (10), formulation (9) can be changed to

$$\begin{aligned}
\min_{\mathbf{w}_m} \quad & ||\mathbf{p}_m(\omega, \theta_{SL}) - \mathbf{w}_m^H \mathbf{S}(\omega, \theta_{SL})||_2 \\
\text{subject to} \quad & \mathbf{w}_m^H \mathbf{S}(\omega, \theta_{ML}) = \mathbf{p}_m(\omega, \theta_{ML}) \\
& \mathbf{w}_m \cdot e^{-j\mathbf{k}_m} = \mathbf{\Gamma}.
\end{aligned} \quad (11)$$

Now we have two sets of un-known variables $\mathbf{w}_m$ and $\mathbf{k}_m$ in the design. To find weight coefficients in (11), we need to find the exact value of $\mathbf{k}_m$; however, $\mathbf{k}_m$ will not be available if $\mathbf{w}_m$ is not obtained first. To solve the dilemma, we consider the following alternating process [31]

1) We first set an initial set of $\mathbf{k}_m$ randomly.
2) With the provided $\mathbf{k}_m$, we can calculate $\mathbf{w}_m$ in (11).
3) The new $\mathbf{k}_m = \angle\mathbf{w}_m$ ($\mathbf{w}_m$ is calculated in step 2) is then used in (11) to update $\mathbf{w}_m$.
4) Repeat step 3) until the cost function in (11) converges.

However, a problem to the above solution is that with the initial random set of $\mathbf{k}_m$, the angle of $\mathbf{w}_m$ will be fixed by

the equality constraint in (11) and will not be able to change during the iterative process. That is, the final set of values of $\mathbf{k}_m$ will be the same as the initial set of $\mathbf{k}_m$. Since the magnitude has been fixed already, the overall result is, the initial value of $\mathbf{w}_m$ calculated in step 2) will also be its final value and no iterative update can be achieved.

To solve the problem so that the angle of $\mathbf{w}_m$ and therefore $\mathbf{w}_m$ itself can converge to the optimal value, we relax the magnitude equality constraint in (10) as follows [32]

$$Re\{\mathbf{w}_m \cdot e^{-j\mathbf{k}_m}\} = \mathbf{\Gamma}, \tag{12}$$

where $Re\{\cdot\}$ represents the real part operator. The above constraint allows $\mathbf{w}_m$ to rotate its angle to meet the other optimisation criteria. As the above iteration is performed step by step, the change of $\mathbf{w}_m$ between adjacent steps will be minimal and therefore $\mathbf{w}_m \cdot e^{-j\mathbf{k}_m}$ is very close to being real-valued and taking their real parts and setting them to fixed real values $\mathbf{\Gamma}$ will only allow a small change of its magnitude. As a result, we can imagine that the magnitude of $\mathbf{w}_m$ will oscillate around the set magnitude values defined by $\mathbf{\Gamma}$ and gradually when it converges, $\mathbf{w}_m \cdot e^{-j\mathbf{k}_m}$ will be real-valued and the final magnitude of $\mathbf{w}_m$ will be the same as set by $\mathbf{\Gamma}$, i.e. all $\mathbf{w}_m$ will have the same magnitude for different m (i.e. different symbols).

Then, DM design in (11) is changed to

$$\min_{\mathbf{w}_m} \quad ||\mathbf{p}_m(\omega, \theta_{SL}) - \mathbf{w}_m^H \mathbf{S}(\omega, \theta_{SL})||_2$$
$$\text{subject to} \quad \mathbf{w}_m^H \mathbf{S}(\omega, \theta_{ML}) = \mathbf{p}_m(\omega, \theta_{ML}) \tag{13}$$
$$Re\{\mathbf{w}_m \cdot e^{-j\mathbf{k}_m}\} = \mathbf{\Gamma}.$$

Based on (13), the iteration process is described as follows:

1) Calculate the values of weight coefficients $\mathbf{w}_m$ in (6).
2) $i = 0$; with $\mathbf{w}_m$ obtained in step 1), calculate $\mathbf{k}_m = \angle \mathbf{w}_m$.
3) $i = i + 1$; at the i-th iteration, with $\mathbf{k}_m$ calculated at the $i - 1$ iteration, we obtain $\mathbf{w}_m$ using (13).
4) Repeat step 3) until the cost function converges.

The above problem (13) can be solved by the CVX toolbox in MATLAB [33, 34].

Note that when $\gamma_0 = \gamma_1 \dots = \gamma_{N-1}$, as derived in [29], γ_n ($n = 0, 1, \dots, N-1$) in $\mathbf{\Gamma}$ has a valid range, and its minimum value is $\frac{|p_m(\omega, \theta_k)|}{N}$, where $|p_m(\omega, \theta_k)|$ represents the desired response in the desired direction θ_k.

IV. DESIGN EXAMPLES

A 40-element uniform linear antenna array (ULA) is employed for directional modulation design. Without loss of generality, we assume there is one mainlobe direction $\theta_{ML} = 60°$ and 163 sidelobe directions with $\theta_{SL} \in [0°, 55°] \cup [65°, 180°]$, sampled every $1°$. The desired response in the mainlobe direction is $\sqrt{2}/2 + \sqrt{2}/2i$, $-\sqrt{2}/2 + \sqrt{2}/2i$, $-\sqrt{2}/2 - \sqrt{2}/2i$ and $\sqrt{2}/2 - \sqrt{2}/2i$ for symbols '00', '01', '11', '10', while the magnitude is fixed to 0.1 with random phase over sidelobe directions. The signal to noise ratio (SNR) is set at 12dB at the desired direction, with the same level of noise for the rest of directions. For the magnitudes of weight coefficients, two design examples are considered. One is a special
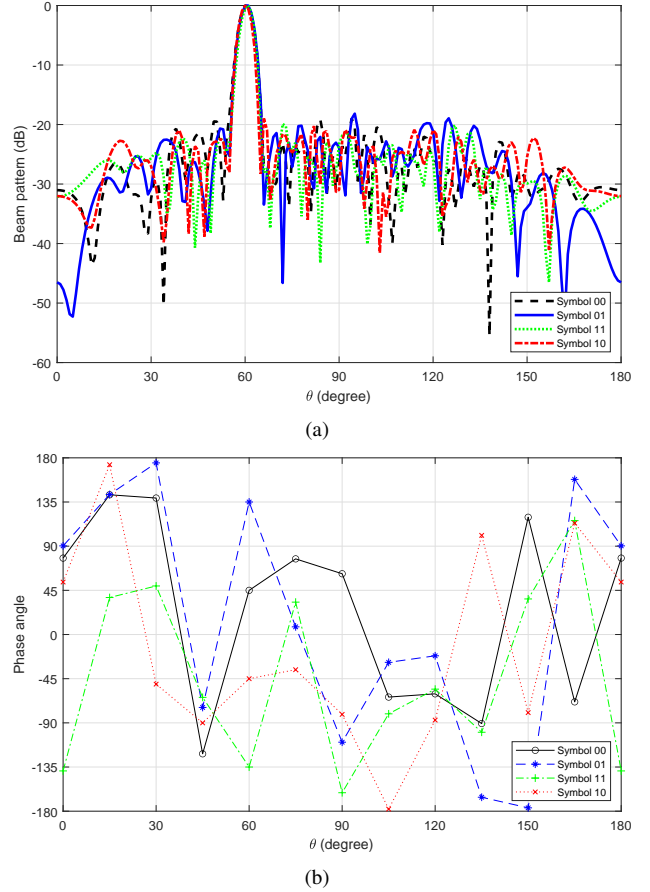

(a)

(b)

Fig. 2. Resultant beam and phase patterns without magnitude constraint using (6).

case where magnitudes for all antennas are the same, i.e. $\gamma_n = 1/38 \approx 0.0263$ ($n = 0, 1, \dots, 39$). The other one is a general example, where coefficient magnitudes for different symbols are the same for the same antenna, but different for different antennas. Here, we assume the symbol-independent random magnitudes for all antennas are between plus or minus 0.01 of $1/30$ ([0.0233, 0.0433]). However, we are not changing the formulation for this design to $0.0233 \leq Re\{\mathbf{w}_m \cdot e^{-j\mathbf{k}_m}\} \leq 0.0433$, as we set $\mathbf{\Gamma}$ as the vector of random values with one specific realization, i.e., the right part of the equality constraint $Re\{\mathbf{w}_m \cdot e^{-j\mathbf{k}_m}\} = \mathbf{\Gamma}$ are a set of specific values randomly generated within the range. In practice, after calibrating the power amplifiers of the radio frequency circuits to the desired value, the real amplification ratio of the circuits could deviate a little bit from that set value due to environmental changes or other factors of the circuits. As a result, it is difficult to keep the RF circuits to always have exactly the same amplification ratio during their practical operations. So the random magnitudes example helps demonstrate the performance of the proposed design in a practical scenario. Note that all the parameters can be determined by designers in advance according to the specific requirements. Design examples with and without the proposed magnitude constraint are provided to show their difference on magnitude values.

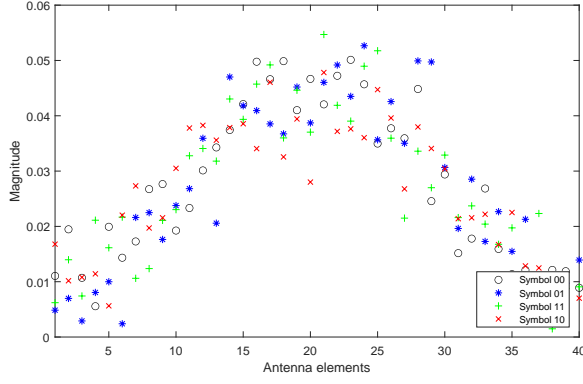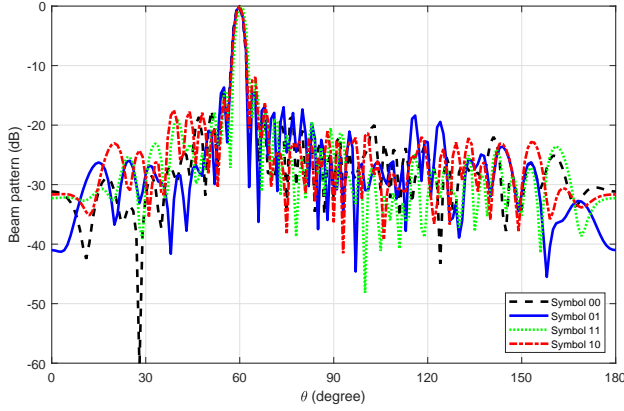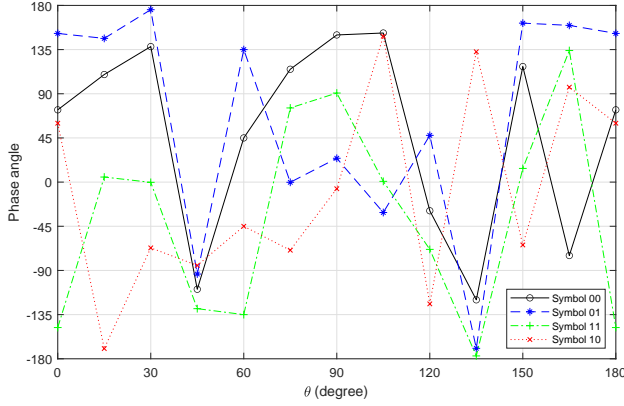The beam and phase patterns without the proposed magni-

Fig. 3. Resultant magnitudes of antenna coefficients without magnitude constraint using (6).

(a)

(b)

Fig. 4. Resultant beam and phase patterns under the same magnitude requirement for all antennas using (13).

tude constraint in (6) are shown in Figs. 2(a) and 2(b), where all main beams are pointed to $\theta = 60°$ (the desired direction) with a low sidelobe level, and the phase in the mainlobe direction are $45°$, $135°$, $-135°$ and $-45°$ for symbols '00', '01', '11', '10', respectively, as required. However, the magnitudes of weight coefficients for all symbols are ranged from 0 to 0.06, as shown in Fig. 3, not meeting the requirement of same magnitude or random magnitude within the range.

For the special case design with both symbol and antenna independent coefficient magnitude, the resultant beam and
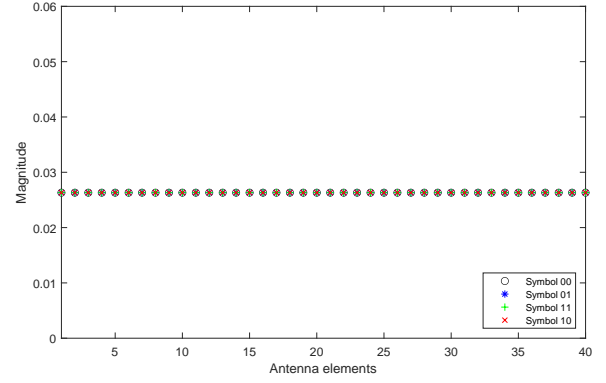

Fig. 5. Resultant magnitudes of antenna coefficients under the same magnitude requirement for all antennas using (13).

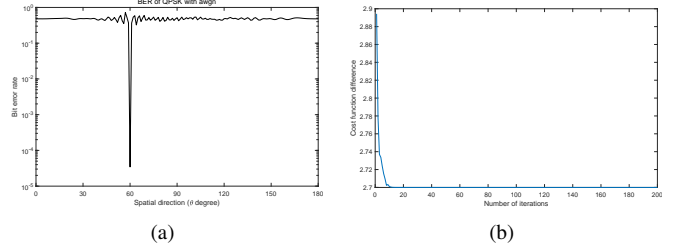
(a)   (b)

Fig. 6. a) BER performance under the same magnitude requirement for all antennas in (13); b) cost function difference under the same magnitude requirement for all antennas in (13).

TABLE I
WEIGHT COEFFICIENTS UNDER THE SAME MAGNITUDE REQUIREMENT
FOR ALL ANTENNAS USING (13).

| n	$w_{0,n}$	$w_{1,n}$	$w_{2,n}$	$w_{3,n}$
0	0.0208 - 0.0162i	-0.0155 - 0.0212i	-0.0206 + 0.0163i	0.0054 + 0.0258i
1	0.0214 + 0.0153i	0.0166 - 0.0204i	-0.0096 - 0.0245i	-0.0138 + 0.0224i
2	-0.0168 + 0.0202i	0.0254 + 0.0068i	0.0211 - 0.0157i	-0.0148 - 0.0218i
3	-0.0262 - 0.0029i	-0.0025 + 0.0262i	0.0029 + 0.0262i	0.0262 + 0.0019i
4	0.0225 - 0.0137i	-0.0147 - 0.0219i	-0.0259 + 0.0049i	0.0198 + 0.0173i
5	0.0221 + 0.0143i	0.0070 - 0.0254i	-0.0173 - 0.0198i	-0.0154 + 0.0213i
6	-0.0174 + 0.0198i	0.0117 + 0.0236i	0.0191 - 0.0181i	-0.0209 - 0.0159i
7	-0.0177 - 0.0195i	-0.0135 + 0.0226i	0.0193 + 0.0179i	0.0135 - 0.0226i
8	0.0190 - 0.0182i	-0.0197 - 0.0174i	-0.0218 + 0.0147i	0.0231 + 0.0125i
9	0.0236 + 0.0117i	0.0128 - 0.0230i	-0.0151 - 0.0216i	-0.0171 + 0.0200i
10	-0.0151 + 0.0216i	0.0147 + 0.0218i	0.0214 - 0.0154i	-0.0207 - 0.0163i
11	-0.0239 - 0.0111i	-0.0156 + 0.0212i	0.0138 + 0.0224i	0.0141 - 0.0222i
12	0.0090 - 0.0247i	-0.0219 - 0.0146i	-0.0243 + 0.0100i	0.0181 + 0.0191i
13	0.0238 + 0.0111i	0.0160 - 0.0209i	-0.0198 - 0.0173i	-0.0098 + 0.0244i
14	-0.0161 + 0.0208i	0.0184 + 0.0188i	0.0154 - 0.0214i	-0.0219 - 0.0146i
15	-0.0185 - 0.0187i	-0.0142 + 0.0222i	0.0153 + 0.0214i	0.0092 - 0.0247i
16	0.0161 - 0.0208i	-0.0141 - 0.0222i	-0.0198 + 0.0174i	0.0194 + 0.0178i
17	0.0236 + 0.0117i	0.0186 - 0.0186i	-0.0168 - 0.0203i	-0.0233 + 0.0122i
18	-0.0228 + 0.0132i	0.0178 + 0.0194i	0.0217 - 0.0149i	-0.0234 - 0.0120i
19	-0.0199 - 0.0172i	-0.0240 + 0.0109i	0.0143 + 0.0221i	0.0105 - 0.0241i
20	0.0192 - 0.0180i	-0.0227 - 0.0133i	-0.0224 + 0.0138i	0.0202 + 0.0169i
21	0.0183 + 0.0189i	0.0230 - 0.0129i	-0.0115 - 0.0236i	-0.0106 + 0.0241i
22	-0.0176 + 0.0196i	0.0225 + 0.0137i	0.0166 - 0.0205i	-0.0152 - 0.0215i
23	-0.0219 - 0.0146i	-0.0191 + 0.0181i	0.0182 + 0.0190i	0.0165 - 0.0205i
23	0.0168 - 0.0202i	-0.0160 - 0.0209i	-0.0125 + 0.0232i	0.0186 + 0.0186i
25	0.0217 + 0.0149i	0.0180 - 0.0192i	-0.0143 - 0.0221i	-0.0105 + 0.0241i
26	-0.0203 + 0.0168i	0.0222 + 0.0141i	0.0196 - 0.0176i	-0.0109 - 0.0239i
27	-0.0178 - 0.0194i	-0.0226 + 0.0134i	0.0191 + 0.0181i	0.0149 - 0.0217i
28	0.0197 - 0.0175i	-0.0211 - 0.0158i	-0.0062 + 0.0256i	0.0197 + 0.0174i
29	0.0103 + 0.0242i	0.0193 - 0.0178i	-0.0238 - 0.0112i	-0.0232 + 0.0124i
30	-0.0239 + 0.0109i	0.0129 + 0.0229i	0.0128 - 0.0230i	-0.0044 - 0.0260i
31	-0.0186 - 0.0186i	-0.0194 + 0.0177i	0.0226 + 0.0134i	0.0210 - 0.0159i
32	0.0214 - 0.0154i	-0.0162 - 0.0208i	-0.0150 + 0.0216i	0.0092 + 0.0247i
33	0.0172 + 0.0200i	0.0204 - 0.0166i	-0.0201 - 0.0170i	-0.0189 + 0.0183i
34	-0.0164 + 0.0206i	0.0060 + 0.0256i	0.0131 - 0.0228i	-0.0219 - 0.0146i
35	-0.0031 - 0.0261i	-0.0250 + 0.0082i	0.0251 + 0.0079i	0.0169 - 0.0202i
36	0.0219 - 0.0145i	0.0023 - 0.0262i	-0.0114 + 0.0237i	0.0240 + 0.0107i
37	-0.0051 + 0.0258i	0.0208 - 0.0162i	-0.0177 - 0.0195i	-0.0244 + 0.0099i
38	-0.0261 - 0.0033i	0.0181 + 0.0191i	0.0083 - 0.0250i	-0.0094 - 0.0246i
39	-0.0232 - 0.0124i	0.0013 + 0.0263i	0.0253 - 0.0072i	0.0254 - 0.0068i
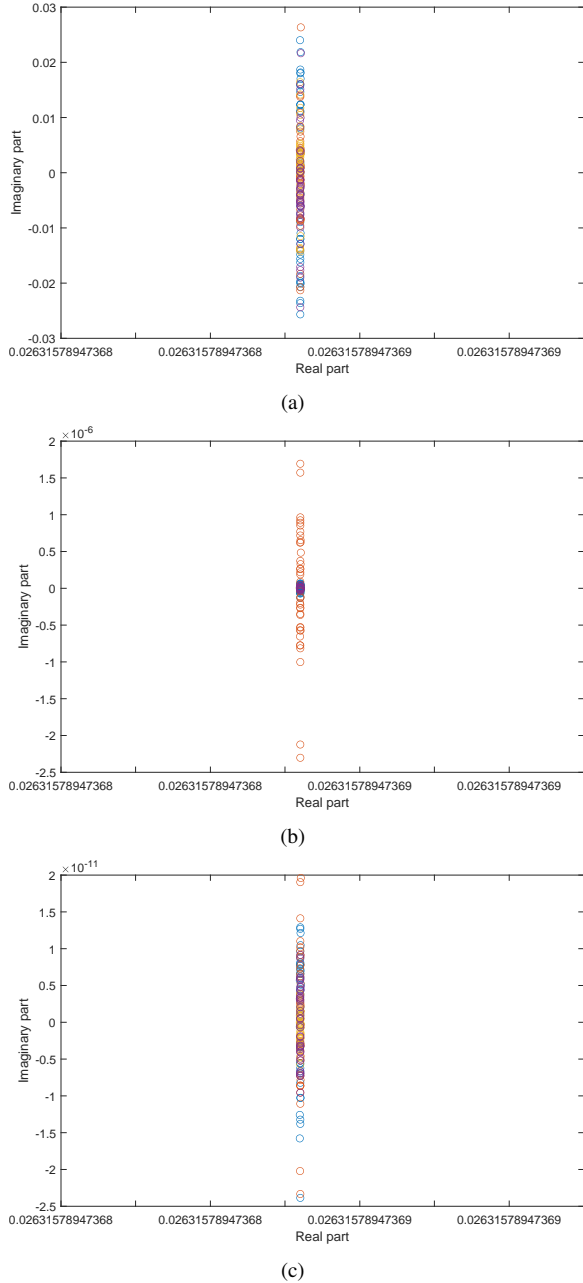
Fig. 7. Real and imaginary parts of $\mathbf{w}_m \cdot e^{-j\mathbf{k}_m}$ under the same magnitude requirement for all antennas at the (a) 1-st, (b) 50-th, (c) 200-th iterations.

phase patterns using (13) are shown in Figs. 4(a) and 4(b), demonstrating a satisfied DM design. As shown in Fig. 5, the magnitudes of weight coefficients at the n-th antenna for all M symbols are the same as $\gamma_n = 1/38$, with the corresponding weight coefficients for all antennas shown in Table I, indicating that the requirement for the same magnitude for all has been achieved. The bit error rates (BERs) at all directions are shown in Fig. 6(a). Here we can see that in un-desired directions the corresponding BER fluctuates around 0.5, while in the desired direction the value is down to 10^{-5}, illustrating the effectiveness of the proposed design. The difference value of cost function has converged, as shown in Fig. 6(b). Fig. 7 shows the convergence process of $\mathbf{w}_n \cdot e^{-j\mathbf{k}_n}$, using Eq. (13)

at the (a) 1-st, (b) 50-th, (c) 200-th iterations. Here we can see that at the first iteration, $\mathbf{w}_m \cdot e^{-j\mathbf{k}_m}$ is a complex number with the imaginary part ranging from [-0.03, 0.03]; while at the 50-th iteration, the real part of $\mathbf{w}_m \cdot e^{-j\mathbf{k}_m}$ is $\frac{1}{38}$, with the value of the imaginary part down to 10^{-6}; and further down to 10^{-11} at the 200-th iteration, demonstrating that with increasing number of iterations, $\mathbf{w}_m \cdot e^{-j\mathbf{k}_m} = Re\{\mathbf{w}_m \cdot e^{-j\mathbf{k}_m}\} = \mathbf{\Gamma}$.

For the general case design with the requirement of the symbol-independent random magnitude for all antennas in the range [0.0233, 0.0433], the resultant corresponding beam and phase patterns in (13) are shown in Figs. 8(a) and 8(b), demonstrating a satisfied DM design. As shown in Fig. 9(a), the magnitudes of weight coefficients at the n-th antenna for all M symbols are within the range, indicating that the requirement of a symbol-independent random magnitude for all antennas has been met. The corresponding weight coefficients for all antennas are shown in Table II. The BERs at all directions are similar to Fig. 6(a), demonstrating the effectiveness of the proposed design. The difference value of cost function in Eq. (13) is shown in Fig. 9(b), where the convergence of cost function can be observed clearly, representing an optimal solution is found. Fig. 10 shows the convergence process of $\mathbf{w}_n \cdot e^{-j\mathbf{k}_n}$. Similar to the design under the both symbol and antenna independent magnitude requirement for all antennas, at the first iteration, $\mathbf{w}_m \cdot e^{-j\mathbf{k}_m}$ is a complex number, with the imaginary part ranging from [-0.03, 0.03]; while at the 50-th iteration, $\mathbf{w}_m \cdot e^{-j\mathbf{k}_m}$ is becoming a real number, as the value of the imaginary part of $\mathbf{w}_m \cdot e^{-j\mathbf{k}_m}$ is down to 10^{-4}; finally, at the 200-th iteration, the value of the imaginary part of $\mathbf{w}_m \cdot e^{-j\mathbf{k}_m}$ is further down to 10^{-8}, with the real part of $\mathbf{w}_m \cdot e^{-j\mathbf{k}_m}$ constrained between 0.0233 and 0.0433, demonstrating again that with increasing number of iterations, $\mathbf{w}_m \cdot e^{-j\mathbf{k}_m} = \Gamma$ can be treated as $Re\{\mathbf{w}_m \cdot e^{-j\mathbf{k}_m}\} = \Gamma$, as the imaginary part of $\mathbf{w}_m \cdot e^{-j\mathbf{k}_m}$ decreases to zero.

V. CONCLUSIONS

With different magnitudes of weight coefficients for different antennas and for different signal symbols, circuits design in analogue implementation would be a challenge. To reduce the implementation complexity, a constant magnitude constraint has been proposed, allowing an effective phase-only control of the directional modulation system, while the amplification ratio of the RF circuits can be fixed. Moreover, different from a previously proposed design, the magnitudes of weight coefficients for all antennas can be chosen by designers in advance according to the specific requirements, allowing more freedom in the design process. The formulation is non-convex and it is transformed into a convex form through iterative optimisation. The proposed physical layer security design has a low implementation complexity and its power consumption can be controlled effectively for low-power applications. All these features make it suitable for 6G enabled IoT, which often requires low complexity and low power and high security. As demonstrated by design examples, with the proposed solution, a symbol independent coefficient magnitude for each antenna can be achieved, while the magnitude for different antennas can be set either the same or not.
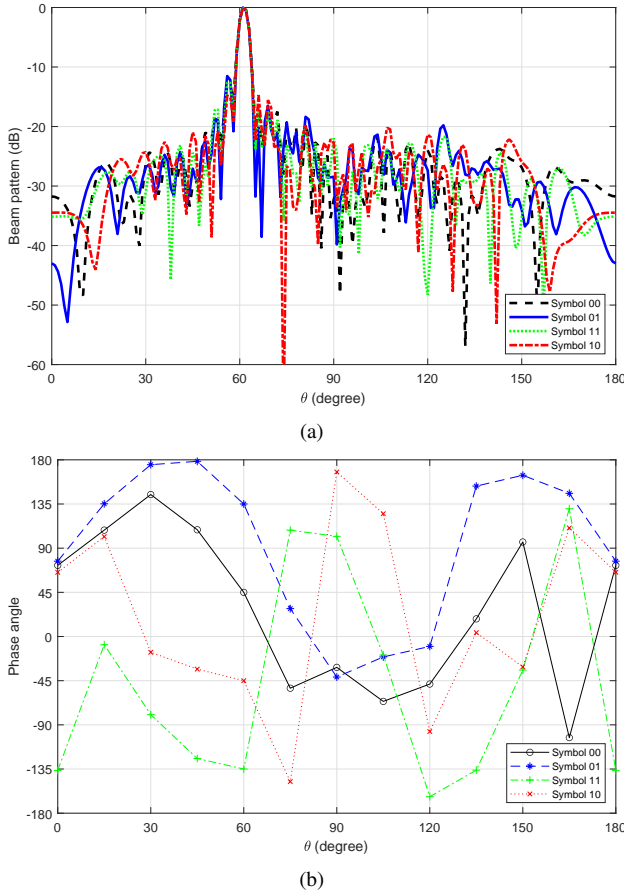
(a)

(b)

Fig. 8. Resultant beam and phase patterns with magnitude constraint under the random magnitude requirement for all antennas within the range [0.0233, 0.0433] in (13).
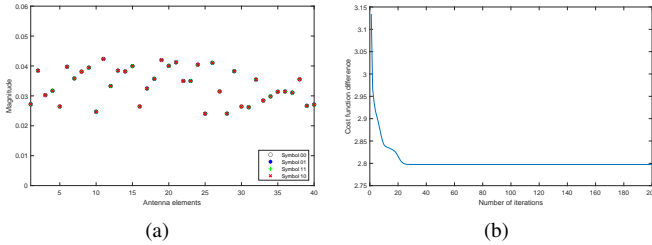

(a)   (b)

Fig. 9. a) Resultant magnitudes of antenna coefficients under the random magnitude requirement for all antennas within the range [0.0233, 0.0433] using (13); b) Cost function difference under the random magnitude requirement for all antennas in the range [0.2333, 0.4333] in (13).

(a)

(b)

(c)

Fig. 10. Real and imaginary parts of $\mathbf{w}_m \cdot e^{-j\mathbf{k}_m}$ under the random magnitude requirement for all antennas in the range [0.2333, 0.4333] at the (a) 1-st, (b) 50-th, (c) 200-th iterations.

REFERENCES

[1] S. Verma, Y. Kawamoto, Z. M. Fadlullah, H. Nishiyama, and N. Kato. A survey on network methodologies for real-time analytics of massive IoT data and open research issues. *IEEE Communications Surveys Tutorials*, 19(3):1457–1477, 2017.

[2] A. Al-Fuqaha, M. Guizani, M. Mohammadi, M. Aledhari, and M. Ayyash. Internet of things: A survey on enabling technologies, protocols, and applications. *IEEE Communications Surveys Tutorials*, 17(4):2347–2376, 2015.

[3] H. Zhu, K. Yuen, L. Mihaylova, and H. Leung. Overview of environment perception for intelligent vehicles. *IEEE Transactions on Intelligent Transportation Systems*, 18(10):2584–2601, 2017, DOI: 10.1109/TITS.2017.2658662.

[4] Hao Zhu, Ke Zou, Yongfu Li, and Henry Leung. Robust sensor fusion with heavy-tailed noises. *Signal Processing*, 175:107659, 2020, DOI: 10.1016/j.sigpro.2020.107659.

[5] S. L. Keoh, S. S. Kumar, and H. Tschofenig. Securing the internet of things: A standardization perspective. *IEEE Internet of Things Journal*, 1(3):265–275, 2014.

[6] P. Huang, Y. Hao, T. Lv, J. Xing, J. Yang, and P. T. Mathiopoulos. Secure beamforming design in relay-

TABLE II

WEIGHT COEFFICIENTS UNDER THE RANDOM MAGNITUDE REQUIREMENT FOR ALL ANTENNAS IN THE RANGE [0.2333, 0.4333] USING (13).

n	$w_{0,n}$	$w_{1,n}$	$w_{2,n}$	$w_{3,n}$
0	0.0272 + 0.0006i	0.0047 - 0.0268i	-0.0272 - 0.0003i	-0.0093 + 0.0255i
1	0.0151 + 0.0353i	0.0383 - 0.0024i	0.0028 - 0.0383i	-0.0380 + 0.0055i
2	-0.0298 + 0.0055i	0.0044 + 0.0299i	0.0300 - 0.0042i	0.0004 - 0.0303i
3	-0.0099 - 0.0301i	-0.0299 + 0.0106i	-0.0050 + 0.0313i	0.0269 + 0.0168i
4	0.0262 + 0.0033i	0.0068 - 0.0256i	-0.0251 - 0.0084i	-0.0101 + 0.0244i
5	-0.0003 + 0.0397i	0.0391 + 0.0071i	-0.0055 - 0.0393i	-0.0394 + 0.0047i
6	-0.0358 + 0.0008i	-0.0079 + 0.0350i	0.0358 - 0.0019i	-0.0075 - 0.0350i
7	-0.0015 - 0.0381i	-0.0375 + 0.0069i	0.0045 + 0.0378i	0.0379 - 0.0035i
8	0.0394 - 0.0016i	-0.0031 - 0.0393i	-0.0392 + 0.0047i	0.0088 + 0.0384i
9	0.0001 + 0.0247i	0.0237 - 0.0068i	-0.0008 - 0.0247i	-0.0245 + 0.0030i
10	-0.0423 + 0.0003i	-0.0049 + 0.0421i	0.0416 - 0.0078i	-0.0090 - 0.0414i
11	-0.0084 - 0.0322i	-0.0318 + 0.0100i	0.0079 + 0.0323i	0.0305 - 0.0132i
12	0.0362 - 0.0128i	-0.0024 - 0.0384i	-0.0384 + 0.0018i	0.0060 + 0.0380i
13	0.0151 + 0.0350i	0.0346 - 0.0161i	-0.0166 - 0.0344i	-0.0346 + 0.0162i
14	-0.0366 + 0.0161i	0.0127 + 0.0379i	0.0318 - 0.0242i	-0.0163 - 0.0365i
15	-0.0094 - 0.0247i	-0.0221 + 0.0146i	0.0116 + 0.0238i	0.0216 - 0.0153i
16	0.0302 - 0.0119i	-0.0077 - 0.0316i	-0.0286 + 0.0154i	0.0144 + 0.0291i
17	0.0229 + 0.0273i	0.0330 - 0.0137i	-0.0151 - 0.0324i	-0.0355 + 0.0033i
18	-0.0403 + 0.0119i	0.0219 + 0.0358i	0.0366 - 0.0206i	-0.0263 - 0.0327i
19	-0.0236 - 0.0323i	-0.0365 + 0.0164i	0.0215 + 0.0338i	0.0273 - 0.0293i
20	0.0334 - 0.0242i	-0.0360 - 0.0201i	-0.0339 + 0.0235i	0.0299 + 0.0284i
21	0.0242 + 0.0252i	0.0275 - 0.0216i	-0.0199 - 0.0288i	-0.0174 + 0.0303i
22	-0.0218 + 0.0274i	0.0328 + 0.0121i	0.0185 - 0.0297i	-0.0228 - 0.0266i
23	-0.0374 - 0.0153i	-0.0184 + 0.0360i	0.0340 + 0.0219i	0.0158 - 0.0372i
24	0.0087 - 0.0224i	-0.0230 - 0.0071i	-0.0071 + 0.0230i	0.0208 + 0.0120i
25	0.0397 + 0.0103i	0.0103 - 0.0397i	-0.0334 - 0.0238i	-0.0085 + 0.0401i
26	-0.0092 + 0.0301i	0.0313 - 0.0033i	-0.0018 - 0.0314i	-0.0299 - 0.0099i
27	-0.0223 - 0.0091i	-0.0114 + 0.0212i	0.0231 + 0.0068i	0.0030 - 0.0239i
28	0.0023 - 0.0382i	-0.0382 - 0.0026i	0.0097 + 0.0370i	0.0376 + 0.0073i
29	0.0249 + 0.0088i	-0.0021 - 0.0263i	-0.0263 + 0.0022i	-0.0096 + 0.0246i
30	0.0009 + 0.0262i	0.0258 - 0.0046i	-0.0032 - 0.0260i	-0.0248 - 0.0086i
31	-0.0350 + 0.0058i	0.0041 + 0.0352i	0.0354 - 0.0021i	-0.0009 - 0.0354i
32	0.0028 - 0.0283i	-0.0268 + 0.0094i	0.0024 + 0.0283i	0.0280 + 0.0049i
33	0.0293 - 0.0056i	0.0012 - 0.0298i	-0.0297 + 0.0020i	0.0061 + 0.0292i
34	0.0090 + 0.0301i	0.0312 + 0.0033i	-0.0052 - 0.0309i	-0.0309 + 0.0054i
35	-0.0314 - 0.0012i	-0.0066 + 0.0308i	0.0266 - 0.0168i	-0.0125 - 0.0289i
36	-0.0073 - 0.0302i	-0.0280 + 0.0134i	-0.0002 + 0.0311i	0.0274 - 0.0147i
37	0.0247 - 0.0255i	-0.0179 - 0.0307i	-0.0331 + 0.0130i	0.0266 + 0.0235i
38	0.0248 + 0.0097i	0.0254 - 0.0080i	-0.0155 - 0.0217i	-0.0267 + 0.0009i
39	-0.0087 + 0.0256i	0.0195 + 0.0189i	0.0155 - 0.0222i	-0.0254 - 0.0096i

assisted internet of things. *IEEE Internet of Things Journal*, 6(4):6453–6464, 2019.

[7] S. H. Chae, C. Jeong, and S. H. Lim. Simultaneous wireless information and power transfer for internet of things sensor networks. *IEEE Internet of Things Journal*, 5(4):2829–2843, 2018.

[8] Z. Deng, Q. Li, Q. Zhang, L. Yang, and J. Qin. Beamforming design for physical layer security in a two-way cognitive radio IoT network with swipt. *IEEE Internet of Things Journal*, 6(6):10786–10798, 2019.

[9] A. Babakhani, D. B. Rutledge, and A. Hajimiri. Near-field direct antenna modulation. *IEEE Microwave Magazine*, 10(1):36–46, February 2009.

[10] M. P. Daly and J. T. Bernhard. Directional modulation technique for phased arrays. *IEEE Transactions on Antennas and Propagation*, 57(9):2633–2640, September 2009.

[11] S. Mufti, A. Tennant, and J. Parrón. Dual channel broadcast using phase-only directional modulation system. In *2018 IEEE International Symposium on Antennas and Propagation USNC/URSI National Radio Science Meeting*, pages 2219–2220, July 2018.

[12] N. Valliappan, A. Lozano, and R. W. Heath. Antenna subset modulation for secure millimeter-wave wireless communication. *IEEE Transactions on Communications*, 61(8):3231–3245, August 2013.

[13] Y. Ding and V. F. Fusco. Directional modulation far-field pattern separation synthesis approach. *IET Microwaves, Antennas Propagation*, 9(1):41–48, 2015.

[14] T. Xie, J. Zhu, and Y. Li. Artificial-noise-aided zero-forcing synthesis approach for secure multi-beam directional modulation. *IEEE Communications Letters*,

PP(99):1–1, 2017.

[15] M. P. Daly and J. T. Bernhard. Beamsteering in pattern reconfigurable arrays using directional modulation. *IEEE Transactions on Antennas and Propagation*, 58(7):2259–2265, March 2010.

[16] T. Hong, M. Z. Song, and Y. Liu. Dual-beam directional modulation technique for physical-layer secure communication. *IEEE Antennas and Wireless Propagation Letters*, 10:1417–1420, December 2011.

[17] Bo Zhang, Wei Liu, Yang Li, Xiaonan Zhao, and Cheng Wang. Directional modulation design under maximum and minimum magnitude constraints for weight coefficients. *Ad Hoc Networks*, 98:102034, 2020.

[18] H. Z. Shi and A. Tennant. Enhancing the security of communication via directly modulated antenna arrays. *IET Microwaves, Antennas & Propagation*, 7(8):606–611, June 2013.

[19] Y. Ding and V. Fusco. Directional modulation transmitter radiation pattern considerations. *IET Microwaves, Antennas & Propagation*, 7(15):1201–1206, December 2013.

[20] Q. J. Zhu, S. W. Yang, R. L. Yao, and Z. P. Nie. Directional modulation based on 4-D antenna arrays. *IEEE Transactions on Antennas and Propagation*, 62(2):621–628, February 2014.

[21] Y. Ding and V. Fusco. A vector approach for the analysis and synthesis of directional modulation transmitters. *IEEE Transactions on Antennas and Propagation*, 62(1):361–370, January 2014.

[22] J. Hu, F. Shu, and J. Li. Robust synthesis method for secure directional modulation with imperfect direction angle. *IEEE Communications Letters*, 20(6):1084–1087, June 2016.

[23] B. Zhang, W. Liu, and Q. Li. Multi-carrier waveform design for directional modulation under peak to average power ratio constraint. *IEEE Access*, pages 1–1, 2019.

[24] B. Guo, Y. Yang, G. Xin, and Y. Tang. Combinatorial interference directional modulation for physical layer security transmission. In *2016 IEEE Information Technology, Networking, Electronic and Automation Control Conference*, pages 710–713, May 2016.

[25] Y. Ding and V. Fusco. Directional modulation transmitter synthesis using particle swarm optimization. In *Proc. Loughborough Antennas and Propagation Conference*, pages 500–503, Loughborough, UK, November 2013.

[26] A. Kalantari, M. Soltanalian, S. Maleki, S. Chatzinotas, and B. Ottersten. Directional modulation via symbol-level precoding: A way to enhance security. *IEEE Journal of Selected Topics in Signal Processing*, 10(8):1478–1493, 2016.

[27] V. F. Fusco and N. B. Buchanan. Retrodirective antenna spatial data protection. *IEEE Antennas and Wireless Propagation Letters*, 8:490–493, 2009.

[28] S. Y. Nusenu, S. Huaizong, Y. Pan, and A. Basit. Directional modulation with precise legitimate location using time-modulation retrodirective frequency diversity array for secure IoT communications. *IEEE Systems Journal*, pages 1–11, 2020.

[29] B. Zhang, W. Liu, Y. Li, X. Zhao, and C. Wang. Di-

rectional modulation design under a constant magnitude constraint for weight coefficients. *IEEE Access*, pages 1–1, 2019.

[30] B. Zhang, W. Liu, and X. Gou. Compressive sensing based sparse antenna array design for directional modulation. *IET Microwaves, Antennas Propagation*, 11(5):634–641, April 2017.

[31] B. Zhang, W. Liu, Q. Li, Y. Li, X. Zhao, C. Zhang, and C. Wang. Metasurface based positional modulation design. *IEEE Access*, 8:113807–113813, 2020.

[32] Q. Li, L. Huang, H. C. So, H. Xue, and P. Zhang. Beampattern synthesis for frequency diverse array via reweighted ℓ_1 iterative phase compensation. *IEEE Transactions on Aerospace and Electronic Systems*, 54(1):467–475, 2018.

[33] M. Grant and S. Boyd. Graph implementations for nonsmooth convex programs. In V. Blondel, S. Boyd, and H. Kimura, editors, *Recent Advances in Learning and Control*, Lecture Notes in Control and Information Sciences, pages 95–110. London, UK. Springer-Verlag Limited, 2008. http://stanford.edu/~boyd/graph$\_$dcp.html.

[34] CVX Research. CVX: Matlab software for disciplined convex programming, version 2.0 beta. http://cvxr.com/cvx, September 2012.

Bo Zhang received his BSc from Tianjin Normal University, China, in 2011. MSc and PhD from the Department of Electrical and Electronic Engineering, University of Sheffield in 2013 and 2018, respectively. He is working with the College of Electronic and Communication Engineering, Tianjin Normal University. His research interests cover array signal processing (beamforming and direction of arrival estimation, etc.), directional modulation, sparse array design and natural language processing.

Wei Liu (S'01-M'04-SM'10) received his BSc and LLB. degrees from Peking University, China, in 1996 and 1997, respectively, MPhil from the University of Hong Kong in 2001, and PhD from the School of Electronics and Computer Science, University of Southampton, UK, in 2003. He then worked as a postdoc first at Southampton and later at Imperial College London. Since September 2005, he has been with the Department of Electronic and Electrical Engineering, University of Sheffield, UK, first as a Lecturer and then a Senior Lecturer. He has published more than 300 journal and conference papers and two research monographs titled "Wideband Beamforming: Concepts and Techniques" (John Wiley, March 2010) and "Low-Cost Smart Antennas" (by Wiley-IEEE, March 2019), respectively. His research interests cover a wide range of topics in signal processing, with a focus on sensor array signal processing and its various applications, such as robotics and autonomous systems, human computer interface, radar, sonar, satellite navigation, and wireless communications.

He is a member of the Digital Signal Processing Technical Committee of the IEEE Circuits and Systems Society (Secretary from May 2020) and the Sensor Array and Multichannel Signal Processing Technical Committee of the IEEE Signal Processing Society (Vice-Chair from Jan 2019). He was an Associate Editor for IEEE Trans. on Signal Processing and currently is an Associate Editor for IEEE Access, and an editorial board member of the journal Frontiers of Information Technology and Electronic Engineering.

Qiang Li received the B.Eng. degree in electronic engineering from the Henan University of Science and Technology, China, in 2010, and the Ph.D. degree in control science and engineering from Harbin Engineering University, China, in 2015. From 2015 to 2016, he was employed at Shenzhen University, China, where he worked on frequency diverse array and space-time adaptive processing. He joined communication group of the University of Sheffield, U.K., in 2016, as a Visiting Scholar, where he researched the phase retrieval algorithms for antenna array. Since 2018, he has been employed at Shenzhen University as an Associate Researcher, where he researched the optimization theory.

Yang Li received B.E. and M.E. degrees from College of Information Technology and Science, Nankai University, Tianjin, in 2008 and 2012, respectively. He received Ph.D. degree from Department of Engineering, Tohoku University, Sendai, in 2017. Currently, he is working at the College of Electronic and Communication Engineering, Tianjin Normal University. His research interests include antenna design, EM-wave propagation, and sensor network.

Xiaonan Zhao received Ph.D. degree from Tianjin University, Tianjin, in 2015. Currently, he is working at the College of Electronic and Communication Engineering, Tianjin Normal University. His research interests include wireless communication channel measurement and modeling.

Cuiping Zhang received M.S.degrees from Tianjin Normal University in 2018. She is working with the College of electronic and Communication Engineering, Tianjin Normal University, Tianjin, China. Her main research interests include wireless sensor networks, image processing.

Cheng Wang received the B.E. degree in measurement and control technology from Xidian University, Xi'an, China, in 2006, the M.E. and Ph.D. degrees in communication engineering and electrical engineering from Nankai University, Tianjin, China, in 2010 and 2014, respectively. From 2012 to 2014, the China Scholarship Council sent him to Columbia University, New York, United States, as a joint training doctoral scholar. During the visiting study, he switched his research interests into condensed matter physics and nanoelectronics. After an interdisciplinary postdoctoral research from 2015 to 2017, in Tsinghua University, Beijing, China, he joined Tianjin Normal University in 2017, as a principal investigator directing the Interdisciplinary Laboratory of Advanced Materials and Devices (X-Lab). His current research interests focus on two-dimensional nanomaterials and devices.